Vol 466|1 July 2010|doi:10.1038/nature09177

ARTICLES

Femtosecond electronic response of atoms to ultra-intense X-rays

L. Young[1], E. P. Kanter[1], B. Krässig[1], Y. Li[1], A. M. March[1], S. T. Pratt[1], R. Santra[1,2], S. H. Southworth[1], N. Rohringer[3], L. F. DiMauro[4], G. Doumy[4], C. A. Roedig[4], N. Berrah[5], L. Fang[5], M. Hoener[5,6], P. H. Bucksbaum[7], J. P. Cryan[7], S. Ghimire[7], J. M. Glownia[7], D. A. Reis[7], J. D. Bozek[8], C. Bostedt[8] & M. Messerschmidt[8]

An era of exploring the interactions of high-intensity, hard X-rays with matter has begun with the start-up of a hard-X-ray free-electron laser, the Linac Coherent Light Source (LCLS). Understanding how electrons in matter respond to ultra-intense X-ray radiation is essential for all applications. Here we reveal the nature of the electronic response in a free atom to unprecedented high-intensity, short-wavelength, high-fluence radiation (respectively 10^{18} W cm^{-2}, 1.5–0.6 nm, $\sim 10^5$ X-ray photons per Å^2). At this fluence, the neon target inevitably changes during the course of a single femtosecond-duration X-ray pulse—by sequentially ejecting electrons—to produce fully-stripped neon through absorption of six photons. Rapid photoejection of inner-shell electrons produces 'hollow' atoms and an intensity-induced X-ray transparency. Such transparency, due to the presence of inner-shell vacancies, can be induced in all atomic, molecular and condensed matter systems at high intensity. Quantitative comparison with theory allows us to extract LCLS fluence and pulse duration. Our successful modelling of X-ray/atom interactions using a straightforward rate equation approach augurs favourably for extension to complex systems.

X-ray crystallography has been the foundation of structural science for the past century. Indeed, almost all the atomic-scale structural knowledge that we have today has been acquired through diffraction within homogeneous crystalline materials. As materials scientists and biologists expand their research to focus more on structure–function relationships, three-dimensional structure determinations of non-periodic and heterogeneous specimens have become increasingly more important, and the use of the fourth dimension, time, becomes central to understanding material structure and dynamics. For this reason, the recent advent of ultrafast, ultra-intense X-rays[1] promises to revolutionize research in structural biology[2], warm dense matter[3,4], femtochemistry[5] and nanoscale dynamics[6].

In biology, approximately 40% of all proteins are not amenable to forming suitable crystals; such proteins include the hydrophobic membrane proteins essential for drug action[7]. The need for crystallization may be eliminated using the method described by Hajdu and collaborators[2]. They proposed that atomic-scale structural information on single biomolecules could be obtained by using high-fluence X-ray pulses of few femtoseconds (1 fs = 10^{-15} s) duration to obtain a diffraction pattern in a single shot before destruction, and thus overcome the conventional damage limit (200 X-ray photons per Å^2)[8]. This principle of single-shot femtosecond diffractive imaging was demonstrated for a micrometre-sized, two-dimensional structure at wavelength $\lambda = 32$ nm (ref. 9), but unoriented three-dimensional complex objects at ångström resolution are only now beginning to be explored. Coulomb explosion of the biomolecule on the 10-fs timescale is typically highlighted as the destruction mechanism of concern. However, even before Coulomb explosion, each atom in the complex undergoes electronic damage—that is, a removal and rearrangement of electrons—that will alter the X-ray diffraction pattern[10]. It is this process of electronic damage, which occurs on femtosecond timescales within a single X-ray pulse, that we investigate here.

Ionization mechanisms

X-ray-induced electronic damage is initiated primarily by photoabsorption[11], with scattering cross-sections being considerably smaller at photon energies below 8 keV for atoms heavier than helium. Thus, the understanding of the photoabsorption mechanism at high X-ray intensity is critical, not only for biomolecular imaging, but also for future studies of chemical, material, condensed matter and plasma systems with X-ray free-electron lasers. At the fluence characteristic of a focused LCLS beam, $\sim 10^5$ X-ray photons per Å^2 per pulse, an atom will absorb multiple photons within a single pulse[12]. As a result, the end of the X-ray pulse probes a target that is entirely different from that existing at the beginning of the pulse. This feature distinguishes X-ray free-electron-laser pulses from synchrotron-radiation pulses, where it is highly unlikely that more than one photon is absorbed during a single pulse because the fluence is typically 10^6 times lower. We are now able to extend studies of X-ray photoabsorption mechanisms to the ultrahigh-intensity, short-wavelength (sub-nanometre) regime. Multiphoton physics in the short-wavelength regime differs considerably from the optical high-intensity regime. In contrast to the optical regime, where even single ionization typically involves many photons, the photons in the X-ray regime carry enough energy for single-photon ionization. In the long-wavelength regime, the availability of high-intensity lasers has permitted detailed studies of the atomic response to near-infrared radiation. Sequential tunnel ionization[13] is the dominant mechanism, leading to multiply-ionized atoms for intensities up to 10^{18} W cm^{-2} (ref. 14).

In the intermediate-wavelength regime ($\sim$10 nm), absorption of a single photon can result in ionization of shallow-core and valence electrons. Photoabsorption mechanisms in this regime have been studied for intensities up to 10^{16} W cm^{-2} using the FLASH free-electron laser[15]. In atomic xenon, multiple ionization up to Xe^{21+} was observed[16]. Sequential single-photon absorption in the early stages of ionization,

[1]Argonne National Laboratory, Argonne, Illinois 60439, USA. [2]The University of Chicago, Chicago, Illinois 60637, USA. [3]Lawrence Livermore National Laboratory, Livermore, California 94551, USA. [4]The Ohio State University, Columbus, Ohio 43210, USA. [5]Western Michigan University, Kalamazoo, Michigan 49008, USA. [6]Lawrence Berkeley National Laboratory, Berkeley, California 94720, USA. [7]PULSE Institute, SLAC National Accelerator Laboratory, Menlo Park, California 94025, USA. [8]Linac Coherent Light Source, SLAC National Accelerator Laboratory, Menlo Park, California 94025, USA.

followed by simultaneous multiphoton absorption, as energetically required to reach the next higher charge state[17], is one proposed mechanism, although the excitation of spectral features such as a giant atomic resonance may modify this simple picture[18]. Studies of high-intensity photoabsorption mechanisms in this wavelength regime have also been conducted on more complex targets[3,19]. For argon clusters, it was found that ionization is best described by sequential single-photon absorption[19] and that plasma effects such as inverse bremsstrahlung, important at longer wavelengths (>100 nm; refs 20, 21), no longer contribute. For solid aluminium targets, researchers recently observed the phenomenon of saturated absorption (that is, a fluence-dependent absorption cross-section) using 15-fs, 13.5-nm pulses and intensities up to 10^{16} W cm^{-2} (ref. 3).

In the short-wavelength regime accessible with the LCLS, single photons ionize deep inner-shell electrons and the atomic response to ultra-intense, short-wavelength radiation ($\sim 10^{18}$ W cm^{-2}, $\sim$1 nm) can be examined experimentally. In contrast to the studies at longer wavelengths, all ionization steps are energetically allowed via single-photon absorption, a fact that makes theoretical modelling considerably simpler. We exploit the remarkable flexibility of the LCLS (photon energy, pulse duration, pulse energy) combined with high resolution electron and ion time-of-flight spectrometers, to monitor and quantify photoabsorption pathways in the prototypical neon atom.

X-ray ionization of neon using LCLS

We chose to study neon because notable changes in the electronic response occur over the initial operating photon energy range of LCLS, 800–2,000 eV (λ = 1.5–0.6 nm), as shown schematically in Fig. 1. There and in the following, V, P and A refer to the ejection of valence, inner-shell and Auger electrons, respectively. In all cases, sequential single-photon ionization dominates, although the differing electron ejection mechanisms lead to vastly different electronic configurations within each ionization stage. The binding energy of a 1*s* electron in neutral neon is 870 eV. For photon energies below this, the valence shell is stripped, as shown at the top of Fig. 1 in a VV… sequence. Above 870 eV, inner-shell electrons are preferentially ejected, creating 1*s* vacancies that are refilled by rapid Auger decay, a PA sequence. For energies above 993 eV, it is possible to create 'hollow' neon, that is, a completely empty 1*s* shell, in a PP sequence if the photoionization rate exceeds that of Auger decay. For energies above 1.36 keV, it is possible to fully strip neon, as shown at the bottom of Fig. 1.

Figure 2a shows experimental ion charge-state yields at three different photon energies, 800 eV, 1,050 eV and 2,000 eV. These photon energies represent the different ionization mechanisms—valence ionization, inner-shell ionization and ionization in the regime far above all edges of all charge stages of neon. Despite the relatively large focal spot for these studies, $\sim$1 μm, the dosage at 2,000 eV for neon (dosage = cross-section × fluence) is comparable to that proposed for the biomolecule imaging experiment where a 0.1-μm focal spot was assumed[2]. At the maximum fluence of $\sim 10^5$ X-ray photons per Å^2, we observe all processes that are energetically allowed via single-photon absorption. Thus, at 2,000 eV, we observe Ne^{10+} and at 800 eV we find charge states as high as Ne^{8+} (a fractional yield of 0.3%), indicating a fully-stripped valence shell. We note that valence stripping up to Ne^{7+} was previously observed in neon for 90.5-eV, 1.8×10^{15} W cm^{-2} irradiation[18,22]. At this intermediate photon energy, 90.5 eV, the highest charge state can not be reached by a sequential single-photon absorption process.

Figure 2b compares the experimental ion charge-state yields with theoretical calculations based on a rate equation model that includes only sequential single-photon absorption and Auger decay processes[12]. For simulations, two parameters are required, the X-ray fluence and pulse duration. The fluence (pulse energy/area) on target may be calculated from measured parameters for pulse energy and focal spot size. The X-ray pulse energies quoted throughout this

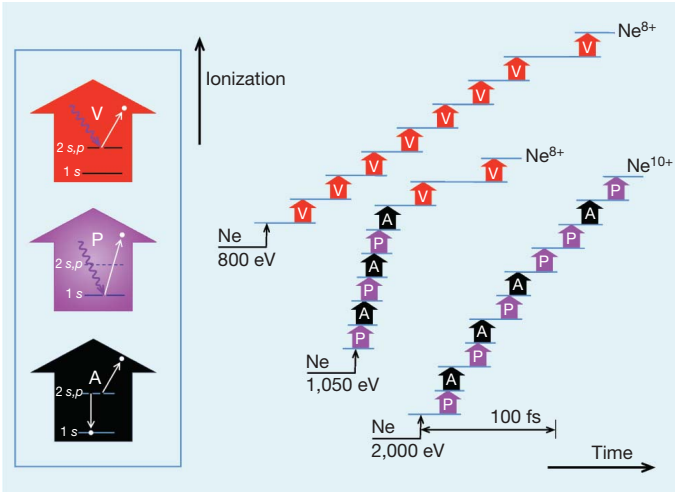

Figure 1 | Diagram of the multiphoton absorption mechanisms in neon induced by ultra-intense X-ray pulses. X-rays with energies below 870 eV ionize 2*s*,*p*-shell valence electrons (V, red arrow). Higher energy X-rays give rise to photoemission from the 1*s* shell (P, purple arrow), and in the consequent Auger decay the 1*s*-shell vacancy is filled by a 2*s*,*p*-shell electron and another 2*s*,*p* electron is emitted (A, black arrow). These V, P and A processes are shown in more detail in the inset; they all increase the charge of the residual ion by one. Main panel, three representative schemes of multiphoton absorption stripping the neon atom. The horizontal direction indicates the time for which atoms are exposed to the high-intensity X-ray radiation field, and vertical steps indicate an increase in ionic charge due to an ionization step, V, P or A. Horizontal steps are approximately to scale with a flux density of 150 X-ray photons per Å^2 per fs, and indicate the mean time between photoionization events or Auger decay.

paper were measured in a gas detector[23] located upstream of the target; the actual pulse energy on target is reduced by five reflections on B_4C mirrors (for details, see Methods). The focal spot size was estimated from measurements done during the commissioning period (J. Krzywinski, personal communication) using the method of X-ray-induced damage craters imprinted in solid targets[24].

The fluence calculated from these pulse-energy and spot-size measurements is corroborated by *in situ* ion-charge-state measurements, both at 800 eV, where ionization is dependent only on fluence and not on intensity, and at 2,000 eV, where the observed ratio of Ne^{10+}/Ne^{9+} resulting from photoionization of hydrogen-like neon (a process with a well-known cross-section) serves as a reliable calibration tool. The fluence that matches the Ne^{10+}/Ne^{9+} ratio agrees to within 30% with that derived from the measured pulse energy (2.4 mJ) and estimated focal spot size ($\sim 1 \times 2$ μm^2 full-width at half-maximum, FWHM) at 2,000 eV. This fluence predicts not only the ratio Ne^{10+}/Ne^{9+}, but also the absolute values of the fractional charge-state yield, as shown in the bottom panel of Fig. 2b. At 2,000 eV, the calculations predict the overall trend of the charge-state yields well, but there are obvious differences—particularly at the lower charge states. The odd–even charge-state alternation is much more pronounced in the calculation than in the experiment. This is due to the fact that the calculation ignores shake-off[25] and double-Auger processes[26], and predicts that 1*s* one-photon ionization produces charge states up to Ne^{2+} only. Experimentally, one observes a yield of $\sim$75% Ne^{2+} and 25% Ne^{3+} from simple 1*s* ionization[27]. At 1,050 eV, the general trends are reproduced although differences due to the simplicity of the model are evident.

At 800 eV, the simulations, which include only valence-shell stripping, are in excellent agreement with the observed charge-state distribution. The fluence, determined *in situ* by the 800-eV data and simulation, is within 10% of that predicted by a $\sim$2.1× increase in focal area when going from 2,000 eV to 800 eV (ref. 28). Here, the simulation is more straightforward as no inner-shell processes are operative. We note that nonlinear two-photon processes[29], which

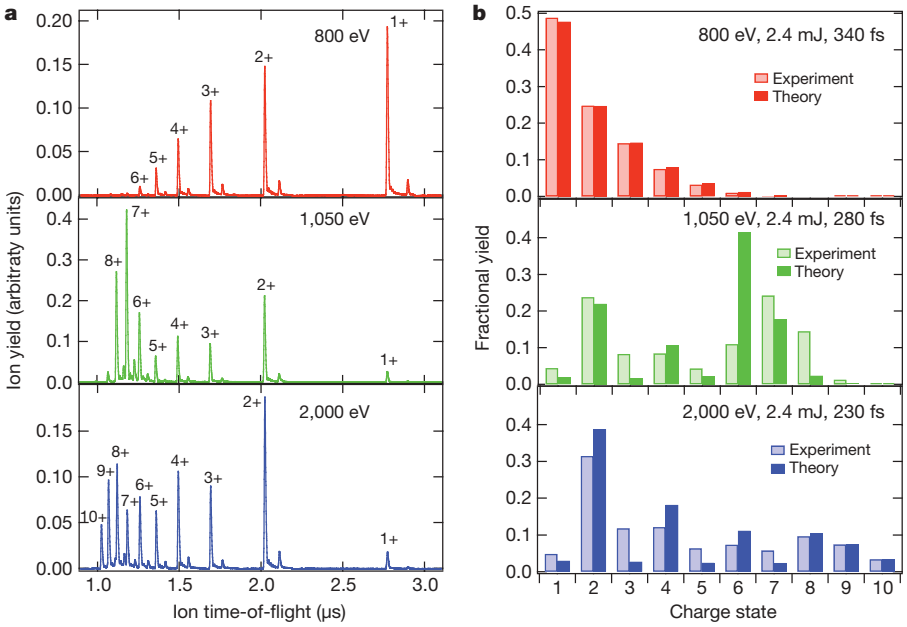

Figure 2 | Neon charge-state yields for X-ray energies below, above and far above the 1s-shell binding energy, 870 eV. Pulse energies are measured in the gas detector upstream of the target. **a**, Experimental charge-state distribution for 2.4-mJ pulses at 800 eV (top), 1,050 eV (middle) and 2,000 eV (bottom). **b**, Comparison of experimental charge-state yields, corrected for detection efficiency, with simulations, assuming a Gaussian-shaped pulse, as described in ref. 12. The X-ray pulse durations for the simulation are assumed to equal the electron bunch duration, shown in the figure. Fluence-dependent processes, such as valence stripping at 800 eV, are insensitive to the pulse duration.

eject an inner-shell electron, are not observed, even at the intensities attained here. Two-photon processes are simply swamped by valence ionization. This observation is consistent with the generalized 1*s* two-photon cross-section of 10^{-55} cm^4 s for neutral neon at 800 eV calculated in ref. 29. For all of these simulations, the X-ray pulse duration was assumed to be equal to the measured LCLS electron bunch duration (230–340 fs)[30].

X-ray transparency

To further investigate photoabsorption mechanisms, we changed the X-ray pulse duration nominally by a factor of ~3, at a fixed pulse energy, for the three photon energies shown in Figs 1 and 2. The spot size of the X-ray beam, imaged upstream of the mirrors, was observed to remain constant to within 10% when changing the pulse duration at a given photon energy—implying a constant focal spot size. At 800 eV and 1,050 eV, we observed essentially no change in the charge-state distribution when changing the pulse duration. However, at 2,000 eV, photoabsorption is markedly decreased with shorter, more intense, X-ray pulses. That is, the sample becomes transparent at high intensity. The phenomenon of intensity-induced X-ray transparency (closely related to saturated absorption[3,31]), can be readily understood qualitatively. Photoabsorption at 2,000 eV is due primarily to the presence of 1*s* electrons. If 1*s* electrons are photoejected by intense X-ray radiation, the absorption cross-section will be decreased—until the 1*s* electrons are replaced by valence electrons. The replacement time is the inner-shell vacancy lifetime. These data are shown in Fig. 3a, where the ratios of the charge-state yields for 230-fs to 80-fs pulses are plotted for 2,000-eV irradiation.

It is more difficult to understand the phenomenon quantitatively. Why would changing the X-ray pulse duration from 230 fs to 80 fs make any difference if Auger decay takes place on a 2.4-fs timescale[32]? The answer is that the Auger refilling time increases dramatically with increasing charge state[33], with a large jump at Ne^{7+}, where the lifetime of a 1*s*-hole state in Ne^{7+} is greater than 23 fs (Fig. 3b). However, even after taking the increased vacancy lifetime into account, our calculations can not reproduce observations if the X-ray pulse durations are taken to be equal to the measured electron bunch durations, that is, 230 fs and 80 fs. The 230-fs simulation agrees well with the measured Ne^{8+} to Ne^{10+} yields at 2,000 eV in Fig. 2b. In order to reproduce the observed transparency, our simulations must therefore use an X-ray pulse duration that is substantially shorter, ~20 fs, for the 80-fs electron bunch. We note that if one incorporates the processes missing from the model[12] (shake and double-Auger), higher charge states will be produced even more rapidly, implying that in the simulation an even shorter pulse duration would be required to reproduce the experimental data. The highly collective process of lasing in a free-electron laser leads to X-ray pulse shapes that need not match the electron current shape, and to the possibility that the X-ray pulse duration could be significantly shorter than the electron bunch duration[34,35].

Hollow-atom signature

Corroborating evidence can be found from electron spectra. Specifically, the production of hollow atoms is sensitive to the pulse duration, as hollow atoms are produced only when the photoionization rate is comparable to the Auger rate. Auger electrons emitted from a double-core-hole state are a distinctive signature of hollow atom formation, with energies shifted well above the single-core-hole Auger electrons. Electron spectra also confirm the validity of the proposed dominant photoabsorption mechanisms—that is, sequential single-photon absorption. Figure 4a and b shows electron spectra at $\theta = 0^\circ$ relative to the X-ray polarization axis for 1,050-eV X-rays. The relatively slow 1*s* photoelectrons are shown in Fig. 4a, whereas the fast valence photoelectrons and Auger electrons are shown in Fig. 4b (where the electron energies have been retarded by 790 eV). The region containing the hollow-atom signature, that is, the double-core-hole Auger, falls between the valence photoelectrons and the single-core-hole Auger. The hollow-atom signature is more cleanly observed at $\theta = 90^\circ$ because the emission of photoelectrons is strongly suppressed perpendicular to the X-ray polarization axis.

The yield of double- versus single-core holes can be derived from an analysis of the electron spectra[36]. The main peaks in the double- and single-core-hole regions were identified as the Auger transitions $[1s^2] \rightarrow [1s\,2p^2]\ ^2D, ^2S$ and $[1s] \rightarrow [2p^2]\ ^1D$, where $[nl]$ represents an nl hole. These main Auger peaks originate from the PPA or PA sequence starting with neutral neon, that is, from the initial stage in the ionization process. Ratios of double-to-single core-hole formation probabilities were derived from the Auger line intensities using

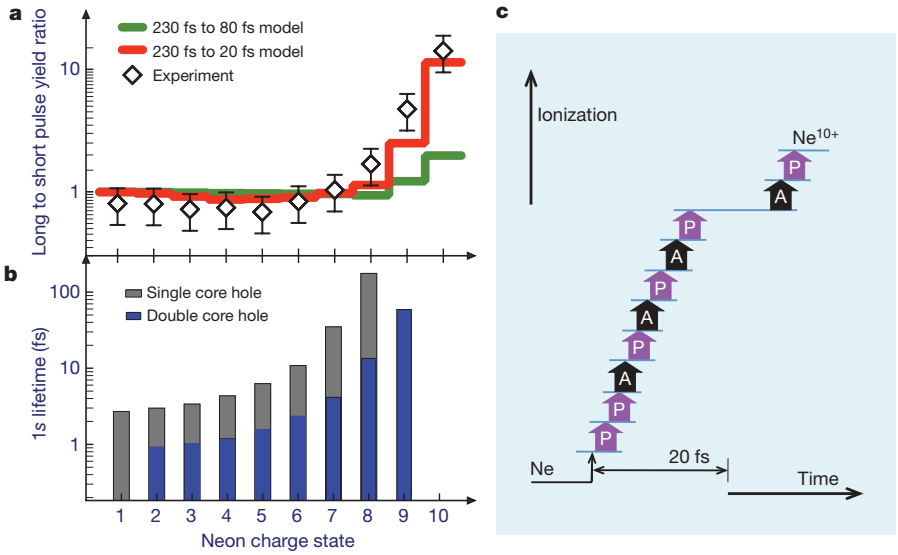

Figure 3 | Intensity-induced X-ray transparency. a, Ratio of charge-state yield for 230-fs to 80-fs electron bunch durations for 2,000-eV, 2.0-mJ X-ray pulses (diamonds). Error bars of ±10% are estimated for the observed charge-state yields. Simulations for 80-fs and 20-fs X-ray pulse durations for the short pulse are overlaid in green and red, respectively. The comparison suggests that the pulse duration of the X-rays generated by the 80-fs electron bunch is less than 80 fs. **b**, Average lifetimes of the single- and double-core-hole states in neon as a function of charge state, from ref. 33. The lifetimes of the single- and double-core holes increase with charge state. These increased lifetimes give rise to a decreased absorption cross-section and hence an intensity-dependent X-ray transparency. The double-core-hole lifetime tracks the observed charge-state ratios. **c**, A scheme leading to high charge states, for a flux density of 2,000 X-ray photons per Å^2 per fs, corresponding to that on target for a 2.0-mJ, 2,000-eV, 20-fs X-ray pulse.

measured and calculated decay rates[37–39]. (We note that this is the first observation of sequential two-photon production of hollow neon atoms and that the yield, ~10%, is ~30× larger than the 0.3% yield—observed in synchrotron radiation studies—that naturally results from electron correlation in the 1*s* shell[36].) The resulting ratios of double-to-single core-hole formation for 1,050-eV X-ray pulses of nominal duration 80 fs are shown in Fig. 5 together with simulations. The simulations for 20 fs and 40 fs form a family from which the observed double-to-single core-hole ratio can be used to estimate the X-ray pulse duration. As is apparent, the X-ray pulse duration appears much shorter than the nominal 80 fs, in agreement with the ion-charge-state transparency data, Fig. 3a. Thus, two independent methods yield the same result—that the nominal ~80-fs mode of operation actually produces X-ray pulses of shorter duration, ~20–40 fs, similar to observations at the FLASH free-electron laser facility[40]. Our observations provide a further example[41] of how ultrafast electronic transitions can be used to characterize X-ray free-electron-laser pulses.

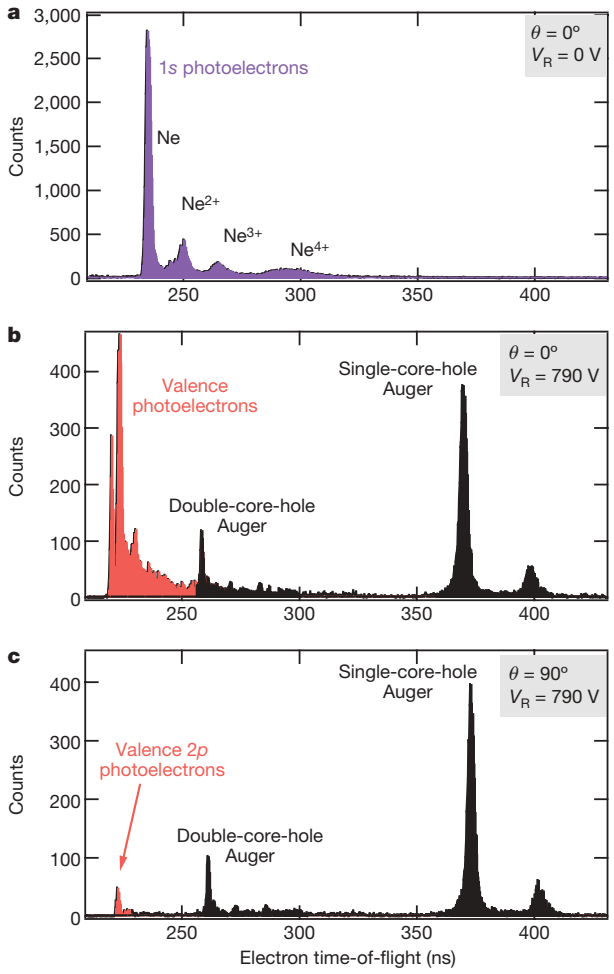

Our observations also provide experimental evidence for the advantageous radiation-hardening effect of using ultra-intense X-ray pulses, and thus have positive implications for proposed single-molecule-imaging experiments[2]. Intense, short X-ray pulses induce transparency via photoejection of both 1*s* electrons to produce hollow atoms. The hollow-atom configuration can be maintained through the ionization process, as sketched in Fig. 3c. As hollow atoms are nominally transparent, the damaging X-ray photoabsorption channel is decreased relative to the imaging (coherent scattering) channel. To be quantitative, the photoabsorption cross-section, σ_{photo}, for hollow neon is decreased 20-fold for 1-Å radiation, that is, to 11 barns, to equal the coherent scattering cross-section, σ_{coh}. This trend of increasing $\sigma_{coh}/\sigma_{photo}$ holds for all hollow atoms. In hollow carbon, $\sigma_{coh}/\sigma_{photo} \approx 2$ for 1-Å radiation, as opposed to ~0.1 for normal carbon. The ideal case

Figure 4 | Electron spectra for inner-shell and valence photoelectrons and Auger electrons created by X-ray pulses at a photon energy of 1,050 eV. a, 1*s* photoelectrons directed along the X-ray polarization axis ($\theta = 0^\circ$) with a photoelectron spectrometer retardation voltage of $V_R = 0$ V. **b**, Valence and Auger electrons at $\theta = 0^\circ$, with $V_R = 790$ V. **c**, Valence and Auger electrons at $\theta = 90^\circ$, $V_R = 790$ V. Auger electrons from double-core-hole states, the signature of hollow atom formation, are more cleanly measured at $\theta = 90^\circ$ (as in **c**), as background from valence ionization is suppressed. The strongest Auger peaks in the double-core-hole and single-core-hole regions originate from the initial PPA and PA ionization sequences, and are used to determine the double-core-hole to single-core-hole formation ratio.

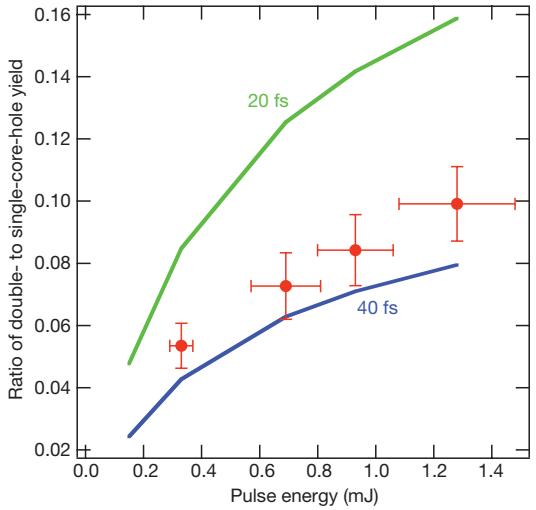

Figure 5 | The ratio of double- to single-core-hole formation as a function of X-ray pulse energy. Red filled circles show experimental data taken with X-rays lasing from an electron bunch of 250 pC charge and 80 fs duration. A gas attenuator was used to reduce the pulse energies. Error bars are statistical ($\pm 1\sigma$) for the Auger yields and measured shot-by-shot X-ray pulse energies. Curves labelled 20 fs (green) and 40 fs (blue) are simulations of the double-to-single core hole formation ratio for two X-ray pulse durations. The comparison suggests that the 80-fs electron bunch generates an X-ray pulse of shorter duration, ~20–40 fs.

for biomolecular imaging is an X-ray pulse shorter than the hollow-atom lifetime, such that scattering occurs before further electron or nuclear dynamics. Experiments on atoms are relevant for single-molecule imaging because hard X-ray interactions are predominantly atomic. For example, plasma effects (such as enhanced absorption via inverse bremsstrahlung) scale as λ^n where $n > 2$ (ref. 42), and are already unimportant at 33 Å (ref. 19) and will be negligible at 1 Å. In addition, collective effects, such as those resulting from the excitation of giant resonances[18], will also be unimportant at photon energies far above all absorption edges.

Conclusions

Our results represent the first observations of photoabsorption mechanisms and femtosecond electronic response in a prototypical atom in the ultra-intense, short-wavelength regime accessed by the LCLS. We find that sequential single-photon absorption dominates, and that with this extreme fluence (10^5 X-ray photons per Å^2) any process that is energetically feasible with a single photon is observed. Thus, the target is continually changing during the course of the femtosecond-duration X-ray pulse. Atoms become transparent at high X-ray intensity owing to the rapid ejection of inner-shell electrons—a phenomenon we call intensity-induced X-ray transparency. The multiple Auger clocks that come into play as the pulse progresses through the atom cause shorter pulses with equal fluence to produce less damage. This concept of multiple clocks extends the standard notion in X-ray experiments of internal clocks on the femtosecond timescale[43]. The transparency is observable in all atomic, molecular[44] and condensed matter systems at high X-ray intensity. Because this study was conducted on the well-characterized neon atom, quantitative comparison with theoretical simulation is possible, and from this comparison we derive measures of LCLS pulse duration and fluence. Finally, the successful modelling of the interaction of ultra-intense X-ray radiation with a free atom using a straightforward rate equation model foreshadows extension of this approach to more complex material systems.

METHODS SUMMARY

The X-ray spectral and pulse characteristics were varied by controlling the electron-bunch energy, charge and compression in the LCLS[30,45,46]. X-ray pulses in the 800–2,000 eV range were focused by Kirkpatrick-Baez mirrors to an estimated $1 \times 2\ \mu m^2$ FWHM in a neon gas jet centred in the AMO (atomic, molecular and optical) instrument[47]. The X-ray pulse energy on target was calculated using the pulse energy measured in upstream gas detectors[22] corrected for the reflectivities of five B_4C mirror surfaces. Ion charge-state spectra were recorded by a time-of-flight analyser. Electron spectra were recorded with five time-of-flight analysers positioned at selected polar and azimuthal angles with respect to the X-ray polarization and propagation directions. Ion charge-state yields were corrected for microchannel plate detection efficiencies[48]. No evidence was observed for charge-changing collisions in ion spectra, nor were space charge effects observable in the electron spectra. A 1-mm slit in the ion-extraction plate limited the length of the X-ray beam observed. The electron spectrometers sampled an estimated length of 1.6 mm. Electron spectrometer efficiencies modelled by Monte Carlo simulation showed good agreement with the measured calibration spectra.

To calculate the atomic response to LCLS pulses, we extended the model described in ref. 12. Using the Hartree-Slater method[49], we determined the subshell photoionization cross-sections for the electron configurations $1s^i\,2s^j\,2p^k$ of Ne^{q+}. Radiative and non-radiative decay rates were taken from ref. 33. The cross-sections and decay rates served as input parameters for rate equations for the populations of the $1s^i\,2s^j\,2p^k$ configurations. We assumed that on average the X-ray temporal pulse profile is Gaussian-shaped. The impact of the longitudinal mode structure is small[12] and was neglected. The charge-state distribution and Auger yields were integrated over the interaction volume, assuming an elliptical Gaussian beam profile.

Full Methods and any associated references are available in the online version of the paper at www.nature.com/nature.

Received 15 February; accepted 10 May 2010.

1. Emma, P. First lasing of the LCLS X-ray FEL at 1.5 Å. In *Proc. 2009 Particle Accelerator Conf.* (IEEE, in the press).
2. Neutze, R., Wouts, R., van der Spoel, D., Weckert, E. & Hajdu, J. Potential for biomolecular imaging with femtosecond X-ray pulses. *Nature* **406,** 752–757 (2000).
3. Nagler, B. *et al.* Turning solid aluminium transparent by intense soft X-ray photoionization. *Nature Phys.* **5,** 693–696 (2009).
4. Lee, R. W. *et al.* Finite temperature dense matter studies on next-generation light sources. *J. Opt. Soc. Am. B* **20,** 770–778 (2003).
5. Gaffney, K. J. & Chapman, H. N. Imaging atomic structure and dynamics with ultrafast X-ray scattering. *Science* **316,** 1444–1448 (2007).
6. Stephenson, G. B., Robert, A. & Grubel, G. Revealing the atomic dance. *Nature Mater.* **8,** 702–703 (2009).
7. Ostermeier, C. & Michel, H. Crystallization of membrane proteins. *Curr. Opin. Struct. Biol.* **7,** 697–701 (1997).
8. Henderson, R. The potential and limitation of neutrons, electrons and X-rays for atomic resolution microscopy of unstained biological molecules. *Q. Rev. Biophys.* **28,** 171–193 (1995).
9. Chapman, H. N. *et al.* Femtosecond diffractive imaging with a soft-X-ray free-electron laser. *Nature Phys.* **2,** 839–843 (2006).
10. Hau-Riege, S. P. X-ray atomic scattering factors of low-Z ions with a core hole. *Phys. Rev. A* **76,** 042511 (2007).
11. Veigele, W. J. Photon cross sections from 0.1 keV to 1 MeV for elements Z=1 to Z=94. *At. Data Tables* **5,** 51–111 (1973).
12. Rohringer, N. & Santra, R. X-ray nonlinear optical processes using a self-amplified spontaneous emission free-electron laser. *Phys. Rev. A* **76,** 033416 (2007).
13. Augst, S., Strickland, D., Meyerhofer, D. D., Chin, S. L. & Eberly, J. H. Tunneling ionization of noble gases in a high-intensity laser field. *Phys. Rev. Lett.* **63,** 2212–2215 (1989).
14. Palaniyappan, S. *et al.* Ultrastrong field ionization of Ne^{n+} ($n \leq 8$): rescattering and the role of the magnetic field. *Phys. Rev. Lett.* **94,** 243003 (2005).
15. Ackermann, W. *et al.* Operation of a free-electron laser from the extreme ultraviolet to the water window. *Nature Photon.* **1,** 336–342 (2007).
16. Sorokin, A. A. *et al.* Photoelectric effect at ultrahigh intensities. *Phys. Rev. Lett.* **99,** 213002 (2007).
17. Makris, M. G., Lambropoulos, P. & Mihelic, A. Theory of multiphoton multielectron ionization of xenon under strong 93-eV radiation. *Phys. Rev. Lett.* **102,** 033002 (2009).
18. Richter, M. *et al.* Extreme ultraviolet laser excites atomic giant resonance. *Phys. Rev. Lett.* **102,** 163002 (2009).
19. Bostedt, C. *et al.* Multistep ionization of argon clusters in intense femtosecond extreme ultraviolet pulses. *Phys. Rev. Lett.* **100,** 133401 (2008).
20. Wabnitz, H. *et al.* Multiple ionization of atom clusters by intense soft X-rays from a free-electron laser. *Nature* **420,** 482–485 (2002).
21. Ziaja, B., Wabnitz, H., Wang, F., Weckert, E. & Möller, T. Energetics, ionization, and expansion dynamics of atomic clusters irradiated with short intense vacuum-ultraviolet pulses. *Phys. Rev. Lett.* **102,** 205002 (2009).
22. Hau-Riege, S. P., Bionta, R. M., Ryutov, D. D. & Drzywinski, J. Measurement of x-ray free-electron-laser pulse energies by photoluminescence in nitrogen gas. *J. Appl. Phys.* **103,** 053306 (2008).

23. Richter, M., Bobashev, S. V., Sorokin, A. A. & Tiedtke, K. Photon-matter interaction at short wavelengths and ultra-high intensity — gas-phase experiments at FLASH. *J. Phys. Conf. Ser.* **141,** 012014 (2008).
24. Chalupsky, J. *et al.* Characteristics of focused soft X-ray free-electron laser beam determined by ablation of organic molecular solids. *Opt. Express* **15,** 6036–6043 (2007).
25. Krause, M. O., Vestal, M. L., Johnson, W. H. & Carlson, T. A. Readjustment of the neon atom ionized in the K shell by X rays. *Phys. Rev.* **133,** A385–A390 (1964).
26. Amusia, M., Ya., Lee, I. S. & Kilin, V. A. Double Auger decay in atoms: probability and angular distribution. *Phys. Rev. A* **45,** 4576–4587 (1992).
27. Saito, N. & Suzuki, I. H. Multiple photoionization of Ne in the K-shell ionization region. *Phys. Scr.* **45,** 253–256 (1992).
28. Barty, A. *et al.* Predicting the coherent X-ray wavefront focal properties at the Linac Coherent Light Source (LCLS) X-ray free electron laser. *Opt. Express* **17,** 15508–15519 (2009).
29. Novikov, S. A. & Hopersky, A. N. Two-photon excitation/ionization of atomic inner shells. *J. Phys. At. Mol. Opt. Phys.* **33,** 2287–2294 (2000).
30. Bane, K. L. F. *et al.* Measurements and modeling of coherent synchrotron radiation and its impact on the Linac Coherent Light Source electron beam. *Phys. Rev. Spec. Top. Accel. Beams* **12,** 030704 (2009).
31. Milonni, P. & Eberly, J. H. *Lasers* (Wiley & Sons, 1988).
32. Krause, M. O. Atomic radiative and radiationless yields for K and L shells. *J. Phys. Chem. Ref. Data* **8,** 307–327 (1979).
33. Bhalla, C. P., Folland, N. O. & Hein, M. A. Theoretical K-shell Auger rates, transition energies, and fluorescence yields for multiply ionized neon. *Phys. Rev. A* **8,** 649–657 (1973).
34. Reiche, S., Musumeci, P., Pellegrini, C. & Rosenzweig, J. B. Development of ultra-short pulse, single coherent spike for SASE X-ray FELs. *Nucl. Instrum. Methods A* **593,** 45–48 (2008).
35. Emma, P. *et al.* Femtosecond and subfemtosecond X-ray pulses from a self-amplified spontaneous-emission-based free electron laser. *Phys. Rev. Lett.* **92,** 074801 (2004).
36. Southworth, S. H. *et al.* Double *K*-shell photoionization of neon. *Phys. Rev. A* **67,** 062712 (2003).
37. Albiez, A., Thoma, M., Weber, W. & Mehlhorn, W. KL_{23} ionization in neon by electron impact in the range 1.5–50 keV: cross sections and alignment. *Z. Phys. D* **16,** 97–106 (1990).
38. Kanngießer, B. *et al.* Simultaneous determination of radiative and nonradiative decay channels in the neon K shell. *Phys. Rev. A* **62,** 014702 (2000).
39. Chen, M. H. Auger transition rates and fluorescence yields for the double-K-hole state. *Phys. Rev. A* **44,** 239–242 (1991).
40. Ayvazyan, V. *et al.* First operation of a free-electron laser generating GW power radiation at 32 nm wavelength. *Eur. Phys. J. D* **37,** 297–303 (2006).
41. Sorokin, A. A. *et al.* Method based on atomic photoionization for spot-size measurement on focused soft x-ray free electron laser beams. *Appl. Phys. Lett.* **89,** 221114 (2006).
42. Krainov, V. P. Inverse stimulated bremsstrahlung of slow electrons under Coulomb scattering. *J. Phys. At. Mol. Opt. Phys.* **33,** 1585–1595 (2000).
43. Föhlisch, A. *et al.* Direct observation of electron dynamics in the attosecond domain. *Nature* **436,** 373–376 (2005).
44. Hoener, M. *et al. Phys. Rev. Lett.* Ultra-intense X-ray induced ionization, dissociation and frustrated absorption in molecular nitrogen. (submitted).
45. Ding, Y. *et al.* Measurements and simulations of ultralow emittance and ultrashort electron beams in the Linac coherent light source. *Phys. Rev. Lett.* **102,** 254801 (2009).
46. Frisch, J. *et al.* in *Proc. BIW08* paper MOIOTIO02, 17–26 (2008); ⟨http://accelconf.web.cern.ch/AccelConf/BIW2008/papers/moiotio02.pdf⟩.
47. Bozek, J. D. AMO instrumentation for the LCLS X-ray FEL. *Eur. Phys. J. Spec. Top.* **169,** 129–132 (2009).
48. Paul, H. & Schinner, A. Empirical stopping power tables for ions from ^{3}Li to ^{18}Ar and from 0.001 to 1000 MeV/nucleon in solids and gases. *At. Data Nucl. Data Tables* **85,** 377–452 (2003).
49. Manson, S. T. & Cooper, J. W. Photo-ionization in the soft x-ray range: Z dependence in a central-potential model. *Phys. Rev.* **165,** 126–138 (1968).

Acknowledgements We thank P. Emma, Z. Huang, R. Iverson, F. J. Decker, J. Frisch, and J. Turner for discussions that allowed us to realize, and subsequently utilize, the flexibility of the LCLS to maximum benefit. We are indebted to the operations staff for the performance of the LCLS in the many modes and energies that we requested throughout the course of this experiment. We thank the software engineers for producing advanced control, data acquisition and analysis capabilities during the experiment. This work was supported by the Chemical Sciences, Geosciences, and Biosciences Division of the Office of Basic Energy Sciences, Office of Science, US Department of Energy (DE-AC02-06CH11357, DE-FG02-04ER15614, DE-FG02-92ER14299). N.R. was supported by the US Department of Energy by Lawrence Livermore National Laboratory (DE-AC52-07NA27344). M.H. thanks the Alexander von Humboldt Foundation for a Feodor Lynen fellowship. P.H.B., J.P.C., S.G., J.M.G. and D.A.R. were supported through the PULSE Institute, which is jointly funded by the Department of Energy, Basic Energy Sciences, Chemical Sciences, Geosciences and Biosciences Division and Division of Materials Science and Engineering. Portions of this research were carried out at the LCLS at the SLAC National Accelerator Laboratory. LCLS is funded by the US Department of Energy's Office of Basic Energy Sciences.

Author Contributions L.Y., R.S., S.H.S., E.P.K. and B.K. conceived the experimental plan, acquired and analysed the data, and wrote the paper. R.S. and N.R. performed the theoretical calculations. J.D.B. and C.B. designed, commissioned and operated the AMO instrument. M.M. assisted during the experiment with upstream X-ray diagnostics. Y.L., A.M.M., S.T.P., L.F.D., G.D., C.A.R., N.B., L.F., M.H., P.H.B., J.P.C., S.G., J.M.G. and D.A.R. contributed to the experiment. All authors contributed to the work presented here and to the final paper.

Author Information Reprints and permissions information is available at www.nature.com/reprints. The authors declare no competing financial interests. Readers are welcome to comment on the online version of this article at www.nature.com/nature. Correspondence and requests for materials should be addressed to L.Y. (young@anl.gov).

METHODS

Experiments. Measurements were made at the LCLS X-ray free-electron-laser facility at the SLAC National Accelerator Laboratory[1,50]. Electron bunches generated at 30 Hz in an RF-photocathode gun were accelerated to 4.2–6.7 GeV and passed through an undulator to produce X-ray pulses in the 800–2,000 eV range by the self-amplified spontaneous emission (SASE) process[51]. The X-ray spectral and pulse characteristics were varied by controlling the electron-bunch charge, energy and compression[30,45,46]. The nominal bunch charge was 250 pC, and two magnetic bunch-compressor chicanes provided control of the bunch length[1,30,46]. Bunch lengths were measured using a transverse RF deflecting cavity to streak the bunch and project it onto a phosphor screen[30,46]. The electron-bunch lengths provide estimates of the durations of the X-ray pulses, but the neon photoionization results suggest that the X-ray pulse durations were shorter than the nominal 80-fs electron bunches at high compression.

Downstream of the undulator, the X-rays pass through a diagnostics section that includes gas and solid attenuators between two gas detectors. The gas detectors are based on photoluminescence in nitrogen gas[23] and provide a signal proportional to the total pulse energy on a shot-by-shot basis. At each X-ray energy used, a procedure was conducted to measure the electron beam energy before and after the undulator (J. Frisch, personal communication). The electron energy loss in the undulator provided a measure of the X-ray pulse energy and absolute calibration of the gas detectors. The pulse energy could be reduced by use of the gas attenuator. This allowed measurements to be made as a function of pulse energy with otherwise identical pulse parameters. As the pulse energies varied if the electron bunch compression was changed, the gas attenuator was also used to make measurements as a function of pulse duration with fixed pulse energy.

X-rays were deflected by three flat mirrors onto two dynamically bent mirrors in Kirkpatrick-Baez (KB) geometry[28,52] that focused the X-rays into the AMO Sciences chamber[47]. The five mirrors are fabricated from polished silicon substrates with B_4C thin-film coatings and are oriented at 14-mrad grazing incidence angles with respect to the X-ray beam. For the three X-ray energies used in these experiments (800 eV, 1,050 eV and 2,000 eV), the calculated reflectivities R for a single mirror are 0.921, 0.931 and 0.898, respectively. After five reflections, the pulse energies are reduced by factors of R^5 from the values measured by the gas detectors, that is, by factors of 0.663, 0.699 and 0.584 at 800 eV, 1,050 eV and 2,000 eV, respectively. These factors assume ideal mirror reflectivities and no other transmission losses. However, a photoionization detector positioned downstream of the KB mirrors subsequently recorded pulse energies only 12–15% of the pulse energies measured with the photoluminescence detectors (A. A. Sorokin *et al.*, personal communication). Those results are a factor of five smaller than the transmission losses owing to mirror reflectivities alone. The KB mirrors are expected to produce a focal spot diameter ~1 μm FWHM[28,52]. The effective focal spot area was determined by measuring the profiles of damage craters imprinted in solid targets (J. Krzywinski, personal communication). The minimum effective spot areas were reported to be $3 \pm 0.7\ \mu m^2$ at 830 eV and $2.5 \pm 0.7\ \mu m^2$ at 2,000 eV.

The focused X-rays passed through a neon gas jet in the AMO chamber[47]. Ion charge-state spectra were recorded by a time-of-flight analyser, and electron spectra were recorded by five time-of-flight analysers positioned at selected polar and azimuthal angles with respect to the polarization and propagation directions of the X-ray beam. Ion charge-state yields were corrected for microchannel plate detection efficiencies that were assumed to be proportional to ion impact velocities[48]. No evidence was observed for charge-changing collisions in the ion spectra, nor were space charge effects significant at the rates the electron spectra were recorded. A slit in the ion extraction plate limited the observed length of the X-ray beam to 1 mm. The electron spectrometers sampled an estimated length of 1.6 mm. Electron spectrometer efficiencies modelled by Monte Carlo simulations showed good agreement with the measured calibration spectra.

The X-ray bandwidth depends on the bunch compression and is roughly estimated as 0.5%. Information on the X-ray bandwidth and jitter could be deduced from the widths of photoelectron lines, although the reported results were not very sensitive to the X-ray energy spread.

Modelling. To calculate the atomic response to LCLS pulses, we extended the model described in ref. 12. Using the Hartree-Slater method[49], we determined the subshell photoionization cross-sections for the electron configurations $1s^i\,2s^j\,2p^k$ of Ne^{q+}. Radiative and non-radiative decay rates were taken from ref. 33. The cross-sections and decay rates served as input parameters for rate equations for the populations of the $1s^i\,2s^j\,2p^k$ configurations. For each set of X-ray pulse parameters, we integrated the rate equations together with equations for the Auger yields. The charge-state distribution and Auger yields were integrated over the interaction volume, assuming an elliptical Gaussian beam profile.

The LCLS is based on the SASE scheme[53,54] and thus provides irreproducible, quasichaotic pulses of highly fluctuating intensity in both the temporal and spectral domains. Each individual SASE pulse consists of a train of phase-uncorrelated intensity spikes of random pulse height and duration[55,56]. These intensity spikes enhance multiphoton processes if the lifetime of the intermediate (virtual) states involved is small in comparison to the coherence time of the SASE radiation. The experimental data shown in this paper were obtained by averaging over many X-ray pulses. It was shown in ref. 12 that for LCLS parameters, the impact of the longitudinal mode structure on averaged data is small. In other words, the temporal structure of the individual pulses is not important. What matters is the average temporal pulse profile, which we assumed to be Gaussian. We also performed calculations using a flat-topped average pulse shape. This had no impact on the charge-state distributions in Figs 2 and 3.

The measured and calculated ion charge-state yields of neon shown in Fig. 2 are sensitive to the X-ray fluence, which is the ratio of pulse energy to focal spot size. Our most reliable comparison of measured and calculated ion yields is at 800 eV, where shake processes not included in the calculations are relatively small (~5%; ref. 57) compared with ~30% shake effects at energies above the 1s ionization threshold[27]. Our results for the fluence can be used to infer the peak pulse energy if the focal spot size is assumed to be known, or vice versa. For example, if we assume an elliptical-Gaussian X-ray beam profile of 1 μm FWHM × 2 μm FWHM in the calculation, we find a good match to the 800-eV ion-yield data if the pulse energy given by the photoluminescence detector is reduced by a factor of $R^5/3$, where R is the mirror reflectivity.

50. McNeil, B. First light from hard X-ray laser. *Nature Photon.* **3**, 375–377 (2009).
51. Bonifacio, R., De Salvo, L., Pierini, P., Piovella, N. & Pellegrini, C. Spectrum, temporal structure, and fluctuations in a high-gain free-electron laser starting from noise. *Phys. Rev. Lett.* **73**, 70–73 (1994).
52. Kelez, N. *et al.* in *Proc. FEL2009* paper WEPC20 546–549 (2009); ⟨http://accelconf.web.cern.ch/AccelConf/FEL2009/papers/wepc20.pdf⟩.
53. Kondratenko, A. M. & Saldin, E. L. Generation of coherent radiation by a relativistic-electron beam in an undulator. *Sov. Phys. Dokl.* **24**, 986–988 (1979).
54. Bonifacio, R., Pellegrini, C. & Narducci, L. M. Collective instabilities and high-gain regime in a free electron laser. *Opt. Commun.* **50**, 373–378 (1984).
55. Saldin, E. L., Schneidmiller, E. A. & Yurkov, M. V. Statistical properties of radiation from VUV and X-ray free electron laser. *Opt. Commun.* **148**, 383–403 (1998).
56. Saldin, E. L., Schneidmiller, E. A. & Yurkov, M. V. *The Physics of Free Electron Lasers* (Springer, 2000).
57. Wuilleumier, F. & Krause, M. O. Photoionization of neon between 100 and 2000 eV: single and multiple processes, angular distributions, and subshell cross sections. *Phys. Rev. A* 10, 242–258 (1974).